Microscopic model for selective permeation in ion channels

Jin Wu
Department of Physiology, University of Rochester Medical Center, Rochester, New York 14642 USA

ABSTRACT Ionic permeation in the selectivity filter of ion channels is analyzed by a microscopic model based on molecular kinetic theory. The energy and flux equations are derived by assuming that: (*a*) the selectivity filter is formed by a symmetrical array of carbonyl groups; (*b*) ion movement is near the axis of the channel; (c) a fraction of water molecules is separated from the ion while it moves across the selectivity filter; (*d*) the applied voltage drops linearly across the selectivity filter; (*e*) ions move independently. Energy profiles, single channel conductances, and the degree of hydration of K^+ in a hypothetical K^+ channel are examined by varying the following microscopic parameters: ion radius and mass, channel radius, number of effective water dipoles, and number of carbonyl groups. The i–V curve is linear up to ±170 mV. If the positions of energy maxima and minima are fixed, this linear range is reduced to ±50 mV. Channel radius and ion-water interactions are found to be two major channel structural determinants for selectivity sequences. Both radius and mass of an ion are important in selectivity mediated by these interactions. The theory predicts a total of 15 possible kinetic selectivity sequences for alkali cations in ion channels with a single selectivity filter.

INTRODUCTION

One of the basic questions in ion channel studies concerns the mechanism by which channels achieve selectivity among different ion species. The rejection of large ions by ion channels can be explained by assuming that at least one restricted region in the pore, the selectivity filter, cuts off the permeation of these ions by their unhydrated ion size (Mullins, 1959; Hille, 1971, 1972, 1973; Bezanilla and Armstrong, 1972). Exclusion of small ions is likely to be related to the dehydration process because the hydration energy of ions is inversely proportional to the unhydrated ion radius (Born, 1920). Therefore, the structural contributions to selectivity include the dimension of the selectivity filter, the electrical field strength of this site, and the strength of ion-water interactions. Analyzing the binding affinity of ion-selective glass electrodes, Eisenman (1962; Eisenman and Krasne, 1975) calculated the electrostatic energies of the ion-water and the ion-site interactions and showed that these alone could account for all 11 equilibrium binding selectivity sequences for alkali metal cations. In this treatment selectivity is determined solely by the ion radius, and not by ion mass. The immediate difficulty of applying binding selectivity theory to ion channels is that the association of the ions with the site achieves only a portion of the ion translocation process in the channel. The high affinity binding side attracts ions and prevents them from leaving the binding site, which leads to a decrease in channel conductance (Bezanilla and Armstrong, 1972). Hille (1975) suggested an extension of Eisenman's theory in which one of the multiple states of a binding site can be alternatively considered as a barrier to avoid the difficulties. Several authors have recognized that ion selectivity of channels not only depends on the size but also the mass of ions in their theoretical approaches (Mackey, 1971; Läuger, 1982; Schröder, 1985*a*, *b*). The dependence on ion mass is supported experimentally by the permeation behavior of a pair of ions that have similar ion radii but distinct ion masses. One example is given by the difference in conductances between K^+ and Tl^+ (Eisenman et al., 1986). Another is indicated by the potent blockade of Ca^{++} current by Cd^{++} (Kostyuk and Krishtal, 1977). A kinetic model able to integrate all above contributing factors, and to predict the possible selectivity sequences in ion channels, has not been available.

A microscopic theory to describe ion selectivity should contain only parameters such as the radius, mass, and valence of ions, and also field strength of the sites (Läuger, 1982). To allow an experimental test of such a theory, it must necessarily be expressed in measurable quantities, e.g., conductance or permeability ratio. Eyring rate theory (ERT), (Parlin and Eyring, 1971; Woodbury, 1971; Läuger, 1973) is a one of the most popular and successful tools in fitting experimental data of ion permeation in channels. Selectivity in this theory is phenomenologically determined by the differences in height of activation energy barriers to the different ion

Address correspondence to Jin Wu, Department of Physiology, University of Rochester Medical Center, 601 Elmwood Avenue, Box 642, Rochester, NY 14642.

0006-3495/91/07/238/14 $2.00

species. The advantage of ERT is that many unknown microscopic parameters are absorbed by a few free constants which can be determined by fitting theoretical results to the experiment data. However, in this approach the molecular mechanism of interactions of an ion with its neighbors is veiled. Selective permeation in classical ERT cannot be solely determined by ion radius and mass without empirical data. The difficulty was partially overcome by modified ERT (Läuger, 1982; Schröder, 1985*a*, *b*) in which the free energy of activation was replaced by the interaction energy and the standard form of the preexponential factor kT/h was replaced by an ion mass-dependent coefficient obtained from the Maxwellian distribution. Use of the preexponential factor kT/h in permeation studies is undesirable also because it overestimates the crossing rate by several orders of magnitude (Cooper et al., 1988). Despite these discrepancies, the experimental data can be successfully fitted by the use of a larger free energy barrier, which offsets the overestimation of this factor (Cooper et al., 1988). This suggests that the correct formulation describing permeation behavior must have the same exponential form of the free energy as in ERT. Molecular kinetic theory, e.g., the Maxwellian and Boltzmann distributions, is a basic microscopic theory that can give rise to an exponential form of interaction energy.

This development of a microscopic model for selectivity has been motivated also by recent advances in molecular biological studies of ion channels. By altering amino acids of acetylcholine channels, it is found that rings of negatively charged amino acids determine the rate of ion transport (Imoto et al., 1988). If the rate-limiting step is at the selectivity filter, then this site might be formed by those rings of charges. In this work I attempt to answer two questions that arise from this hypothesis. Firstly, if a ring of charges is in fact found at the selectivity filter, can we characterize ion permeation? Secondly, can we determine the possible selectivity sequences? Further, the answers to these questions may be useful in interpreting or predicting the permeation behavior resulting from modifications of the selectivity filter that are achieved through site-directed mutagenesis. A brief report of the present work has appeared in abstract form (Wu, 1991).

THEORY

The exact three-dimensional structure of the selectivity filter of most channels is not yet available. To explore the selective permeation at the molecular level, a simple structural model consistent with current knowledge of channel structures is proposed, as shown schematically in Fig. 1 *A*. The following five basic assumptions are essential in simplifying the energy equation and the kinetic model. First, the selectivity filter of an ion channel is formed by an axially symmetric ring of multiple carbonyl (CO) groups. Second, the ion movement is constrained to be near the axis of the selectivity filter. Third, only a small fraction of water molecules can move across the selectivity filter with the ion. Thus, at the moment of translocation across the selectivity filter the ion is separated from though still attracted by the remaining fraction of water dipoles in its vicinity. These separated water dipoles (WD) are idealized by an effective dipole (p) representing the axial component of the interaction at either side of the selectivity filter. Fourth, the applied voltage drop in the region of the selectivity filter is linear. Fifth, ion movement within the channel is independent of other ions.

The total interaction energy of ion with sites, water

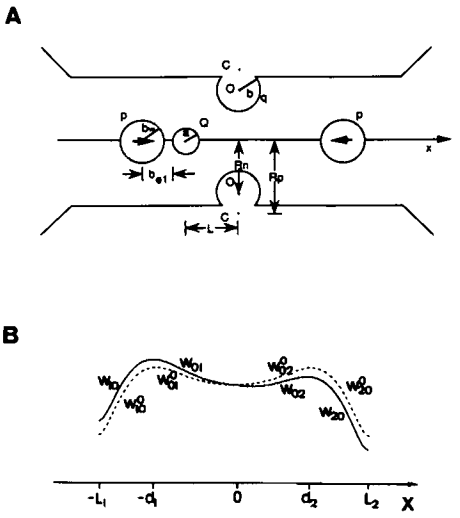

FIGURE 1 (*A*) A schematic diagram of the proposed model of a selectivity filter. Q, the charge of ion; a, the ion radius; O, the carbonyl oxygen; C, the carbonyl carbon; b, the Van der Waals' radius of carbonyl oxygen; R_n, the distance from the carbonyl oxygen to the channel axis (x); R_p, the distance from the carbonyl carbon to the channel axis; q, the equivalent charge on carbonyl oxygen/carbon; p, the effective water dipole; b_w, Van der Waals' radius of water; b_{e1}, the effective water radius; L, the distance for the ion to be separated from the effective water dipoles. (*B*) The typical energy profiles generated from the model. The dashed line is the total interaction energy without external field; the solid line is the profile with applied 25 mV voltage across the selectivity filter. $-L_1$ and L_2, the positions at side 1 and side 2, respectively, where the ion begins the separation from the effective water dipoles; $-d_1$ and d_2, the peak positions at side 1 and side 2, respectively; W_{10}, the energy barrier from side 1 to the center (0 on the x-axis); W_{01}, the energy barrier from center to side 1. W_{02}, the energy barrier from the center to side 2; W_{20}, the energy barrier from side 2 to the center; the energy with superscript 0 corresponds to the same barrier with a zero external field.

dipole, and external fields, $W(x)$, is derived as follows:

$$W(x) = -\frac{QVx}{2L} + \frac{Q}{4\pi\epsilon_0}\left[\frac{q}{\sqrt{x^2+R_p^2}} - \frac{q}{\sqrt{x^2+R_n^2}} - \frac{p}{(L+a+b_{e1}+x)^2} - \frac{p}{(L+a+b_{e2}-x)^2}\right] + \frac{qQ}{48\pi\epsilon_0}\frac{(a+b)^{11}}{(x^2+R_n^2)^6} + \frac{pQ(a+b_w)^{10}}{24\pi\epsilon_0} \cdot \left[\frac{1}{(L+a+b_{e1}+x)^{12}} + \frac{1}{(L+a+b_{e1}-x)^{12}}\right], \quad (1)$$

where, a = crystal radius of ion; b = Van der Waals' radius of carbonyl oxygen; b_{e1}, b_{e2} = effective water radius at either side of the selectivity filter; b_w = Van der Waals' radius of a water molecule; ϵ_0 = permittivity in free space; L = distance from the channel center along the x-axis, where the ion begins to separate from the effective water dipoles; p = effective water dipole moment; q = equivalent charge of site carbonyl oxygen or carbon; Q = charge of ion; R_n = distance from the carbonyl oxygen center to the center of the selectivity filter; R_p = distance from the carbonyl carbon center to the center of the selectivity filter; V = voltage across $-L$ and L; x = coordinate along the channel axis.

The first term of the above equation is the interaction energy of the external field with the ion, in which the energy zero is chosen at coordinate zero. The second term is the electrical interaction energy due to the carbonyl groups and the effective water dipoles. The carbonyl oxygen (O) and carbon (C) are idealized as point charges (q); each carries -0.44 or 0.44 unit of basic charge. The effect of ion-water attraction is represented by an effective dipole (p) placed along the channel axis and oriented toward the ion. The third and fourth terms are the short-range repulsive interactions of carbonyl oxygens with the ion and those of water oxygens with the ion. The power of the repulsive term ranges from 6 to 12 in ionic crystals (Seitz, 1940). In this work, the twelfth power is used and the ninth power is also discussed in Results. The force constants (coefficients of terms 3 and 4) were determined by minimizing the isolated interactions between the ion and the selected object in free space. With the presence of carbonyl group and external field the effective equilibrium water radius b_{e1} at side 1 or b_{e2} at side 2 is no longer equal to the Van der Waals' radius of the water (b_w) and has to be recalculated by minimizing the total interaction energy:

$$\left.\frac{dW(x)}{dx}\right|_{x=-L,\text{ or } x=L} = 0. \quad (2)$$

Eq. 2 was solved numerically by varying b_{e1} and b_{e2} for each set of parameters. Initially b_{e1} is set equal to b_{e2} and the ion is located at $-L$. b_{e1} is varied until $W(-L)$ is minimized. Then with the ion fixed at L, b_{e2} is varied to minimize $W(L)$. The minimization procedure insures that the ion is at equilibrium at $x = -L$ and $x = L$, where the ion and the effective water dipoles begin to separate.

The typical energy profile generated by Eq. 1 has two barriers and one well which is illustrated as the solid line in Fig. 1 *B*. The minimum velocity for ion species A to pass over the first barrier W_{10} from side 1 to side 2 is:

$$u_{min} = \sqrt{\frac{2W_{10}}{m_A}}, \quad (3)$$

where m_A is the mass of ion A.

Integrating the Maxwellian velocity distribution and using Eq. 3, the rate per unit area of ions passing over the barrier W_{10} is:

$$\int_{u_{min}}^{\infty} A_1 \sqrt{\frac{m_A}{2\pi kT}} e^{-m_A u^2/2kT}\, u\, du = \frac{1}{4} A_1 v_A e^{-W_{10}/kT}, \quad (4)$$

where

$$v_A = \sqrt{\frac{8kT}{\pi m_A}} \quad (5)$$

is the average speed of ion A. A_1 is the concentration of ion A at side 1, k is the Boltzmann constant, and T is the absolute temperature. The partition coefficient here is considered to be unity for simplicity.

Assume ion A can reach a quasiequilibrium state and has a very short dwell time in the central energy well. According to the Boltzmann distribution, the probability for ion A to pass over the second barrier W_{02} is $\exp[-W_{02}/kT]$. Then the unidirectional single channel flux equation is obtained from Eq. 4:

$$j_{1A} = \tfrac{1}{4} A_1 S_{1A} v_A e^{-W_{10}/kT} e^{-W_{02}/kT} \quad (6)$$

similarly,

$$j_{2A} = \tfrac{1}{4} A_2 S_{2A} v_A e^{-W_{20}/kT} e^{-W_{01}/kT}, \quad (7)$$

where A_1 and A_2 are the concentrations of ion A at side 1 and side 2, respectively. S_{1A} and S_{2A} are the maximum cross-sectional areas of the selectivity filter to ion A at side 1 and side 2, which are defined by $\pi(R_n - a)^2$.

The single channel current equation is obtained from Eq. 6 and Eq. 7:

$$i_A = \tfrac{1}{4} Q v_A [A_1 S_{1A} e^{-(W_{10}+W_{02})/kT} - A_2 S_{2A} e^{-(W_{20}+W_{01})/kT}]. \quad (8)$$

Fig. 1 *B* illustrates the changes of energy profiles with a weak applied external electrical field. The dashed line is the energy profile of an ion in a channel with zero external field. The solid line is that with applied 25 mV

between $-L_1$ and L_2. Assume the channel is symmetric in both cross-sectional area ($S_{1A} = S_{2A}$) and distance of separation ($L_1 = L_2 = L$). Then, $W^0_{10} = W^0_{20} = W^0$ and $W^0_{01} = W^0_{02} = W^0_0$ (symmetric zero voltage energy barrier). Although in general both the peak positions and the well positions are voltage dependent, I shall consider the changes in these positions to be small under the condition of a weak external field. Then, $d_1 = d_2 = d$ and the well position remains at 0. The single channel current equation, Eq. 8, is expressed as a function of voltage:

$$i_A = \tfrac{1}{4} Q v_A S_A e^{-(W^0 + W^0_0)/kT} [A_1 e^{QV/2kT} - A_2 e^{-QV/2kT}]. \quad (9)$$

For symmetric solutions at side 1 and side 2 ($A_1 = A_2 = A$), Eq. 9 can be further simplified:

$$i_A = \frac{1}{2} Q v_A A S e^{-(W^0 + W^0_0)/kT} \sinh\left(\frac{QV}{2kT}\right). \quad (10)$$

At equilibrium ($i_A = 0$) Eq. 9 can be reduced to the Nernst Equation. If the permeability is defined by:

$$P_i = \tfrac{1}{4} v_i S_i e^{-(W^0_i + W^0_{0i})/kT}, \quad i = A, B, C \ldots . \quad (11)$$

then for two monovalent cation species A and B, the current Eq. 9 with Eq. 11 can be written as:

$$i = QP_A(A_1 e^{QV/2kT} - A_2 e^{-QV/2kT}) + QP_B(B_1 e^{QV/2kT} - B_2 e^{-QV/2kT}). \quad (12)$$

In the steady state ($i = 0$), the Goldman-Hodgkin-Katz (GHK) equation (Goldman, 1943; Hodgkin and Katz, 1949) is obtained from Eq. 12:

$$V = \frac{kT}{Q} \ln \frac{P_A A_2 + P_B B_2}{P_A A_1 + P_B B_1}. \quad (13)$$

The permeabilities in Eq. 13 as defined in Eq. 11 are functions of microscopic parameters only and are voltage and concentration independent. Permeability can be experimentally determined from Eq. 9 or Eq. 10.

The energy profiles shown in Fig. 1 *B* may alternatively have one or three peaks depending on the channel parameters, as will be shown in Results. The situation with one peak is the special case of that of two peaks where $W^0_0 = 0$. For three peaks, repeating the above derivation procedure, the same formulations can be obtained, except that in the definition of the permeability the energy of the third barrier is added to the exponential part of the energy term.

Since all ion channels exhibit ion–ion interactions indicated by saturation, the assumption of independence in the model may cause errors. I have evaluated the effect of ion–ion interactions and found that in symmetrical solutions if the concentration is low, including ion–ion interactions does not significantly improve the precision of the results but adds much more complexity. On the other hand, if a second ion species is introduced in the solution, the ion–ion interactions are prominent and the results deviate from independence markedly. I also found that the permeabilities obtained from biionic reversal potentials are dependent upon ionic strength, mole fraction, and species of reference ions. When two ion species are present, the permeability ratio is often used to characterize channel selectivity. However, the above complications make use of this parameter difficult here. Further, the situation of symmetrical solutions and low applied voltage is closer to the quasiequilibrium condition as required by Maxwellian and Boltzmann distributions (see Discussion). For these reasons, throughout the present work, ion permeation and selectivity are represented by the single channel conductance, which is measured with symmetrical solutions of low concentrations, and with an applied potential difference of 10 mV. The reversal potential, which may be more easily measured experimentally, is not employed here to describe selectivity.

It should be mentioned that the term conductance as used in this work includes only the contributions of the selectivity filter. In actual channels the access resistance should be taken into consideration. The image potentials exerted by the low dielectric medium of the hydrocarbon around the channel wall may affect ions by their valences and offset the conductances for all alkali metal cations. However, this potential is unlikely to discriminate among alkali metal cations by their size. To focus the present study on selectivity and keep the formulation simple, the image potential is excluded from the energy function. While ions enter the channel mouth, they may undergo an initial stage of dehydration, losing their outermost hydration layer. If the "selectivity filter" is not very restrictive, this phase may well be a rate-limiting step. I again consider that this step poorly discriminates among alkali metal cations.

RESULTS

Components of the total energy profiles

Fig. 2 illustrates each component of the total energy profile of K^+ in a hypothetical K^+ channel calculated from Eq. 1. The parameters used are listed in Table 1. Unless otherwise noted, these parameters were used in all calculations. Curve 1 in Fig. 2 is the interaction energy of the voltage drop between $-L$ and L. It is linear and is zero at coordinate zero on the x-axis. Curve 2 is the Coulombic contribution of carbonyl groups which is negative and long range. Curve 3 is the summation of the

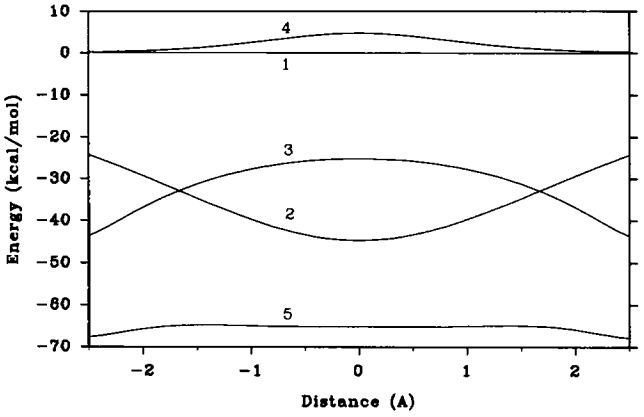

FIGURE 2 The total interaction energy and its components for a K^+ ion in a hypothetical K^+ channel, calculated by Eq. 1. 10 mV is applied across $-L$ and L. Curve 1 is the energy of the external field. Curve 2 is the Coulombic interaction energy of the site carbonyl groups. Curve 3 is the sum of the ion-dipole and the short-range interaction energy between the water dipoles and the ion. Curve 4 is the short-range interaction energy between the site carbonyl groups and the ion. Curve 5 is the total interaction energy of the ion, the sum of all other curves.

effective water dipole interactions and short-range interactions between water and the ion. This energy can be considered as the dehydration energy for the ion crossing the selectivity filter. Curve 4 is the short-range interaction energy of carbonyl oxygens and the ion. It is positive, thus acting as a repulsive force. Curve 5 is the total interaction energy of the ion, i.e., the summation of all the above components. The total energy was minimized at $x = -2.5$ Å and at $x = 2.5$ Å by varying b_{e1} and b_{e2}. There are two peaks and one well in this energy profile. The negative energy (curve 2) of the carbonyl groups reduces the height of the total energy barrier thus effectively compensating the dehydration energy (curve 3). The difference in the height between the two peaks is contributed by the applied voltage across $-L$ and L (curve 1).

TABLE 1 **Parameters**

Parameter	Value	Units
a_K	1.33	*Å*
A_1, A_2	100	*mM/l*
b	1.40	*Å*
b_w	1.56	*Å*
ϵ_0	8.85×10^{-12}	*farad/m*
L	2.5	*Å*
m_K	39.1	*g/mol*
R_n	2.976	*Å*
R_p^*	4.276	*Å*
V	10	*mV*
q	3	*CO*‡
p	3	*WD*§
Q	1.6×10^{-19}	*C*

*Bond length of carbonyl group, $R_p - R_n = 1.3$ Å.
‡Carbonyl groups; 1 CO = 0.44 electron charge (see Eisenman, 1975).
§Effective water dipoles; 1 WD = 6.24×10^{-30} coulomb m.

Effects of ion radius and mass on energy profiles, conductances, and hydrations

Fig. 3 *A* shows the energy profiles of Li^+, Na^+, K^+, Rb^+, and Cs^+ in a hypothetical K^+ channel calculated by Eq. 1. For these cations: $a_{Li} = 0.60$ Å, $a_{Na} = 0.95$ Å, $a_K = 1.33$ Å, $a_{Rb} = 1.48$ Å, $a_{Cs} = 1.69$ Å, $m_{Li} = 6.94$ g/mol, $m_{Na} = 23.0$ g/mol, $m_K = 39.1$ g/mol, $m_{Rb} = 85.5$ g/mol, $m_{Cs} = 132.9$ g/mol (see Hille, 1984). All other parameters are identical to the above set. The R_n (2.976 Å) is finely adjusted to allow the channel conductance of K^+ to exceed that of Rb^+. The total energy was minimized at $x = -2.5$ Å and $x = 2.5$ Å. The height of the first peak which reflects the compensated dehydration energy from side 1 to side 2 is 21.12, 8.83, 2.81, and 3.49 kcal/mol for the Li^+, Na^+, K^+, and Rb^+, respectively. The central well produced by the carbonyl oxygens is gradually shallower as the radius of the ion increases and becomes a peak for Rb^+ and Cs^+ due to the increase in short-range repulsions of larger ions. The single central peak for Cs^+ is 10.14 kcal/mol from side 1 to side 2. The bottom panel in Fig. 3 *B* shows the corresponding chord conductances versus the radius of ions for the above energy profiles calculated from Eq. 8 with 10 mV. The conductances for Li^+, Na^+, K^+, Rb^+, and Cs^+ are 4.5×10^{-12}, 4.4×10^{-4}, 14.7, 4.2, and 3.5×10^{-5} pS, respectively. Fig. 3 *B* (*top*) shows the effective water radius at side 1 (b_{e1}) versus the radius of ions. The effective equilibrium water radius increases at higher ionic radii, indicating that water dipoles are bound less tightly. Fig. 3 *C* shows the conductance of hypothetical ions with a radius of 1.33 Å and molecular weight varying from 10 to 250 g/mol. The conductance hyperbolically decreases as the molecular weight increases. The energy profiles for alkali cations in Fig. 3 *A* depend on the ion radius but not the ion mass according to Eq. 1. Fig. 3 *C* shows that conductance is influenced by ion mass as well.

Field strength of the sites compensates for dehydration energy

The energy profiles in Fig. 4 *A* represent the total energy of K^+ in a hypothetical K^+ channel calculated from Eq. 1. The total energy was minimized at $x = -2.5$ Å and $x = 2.5$ Å. The number of carbonyl (CO) groups was varied from 2 to 4. For the situation of two CO groups, the

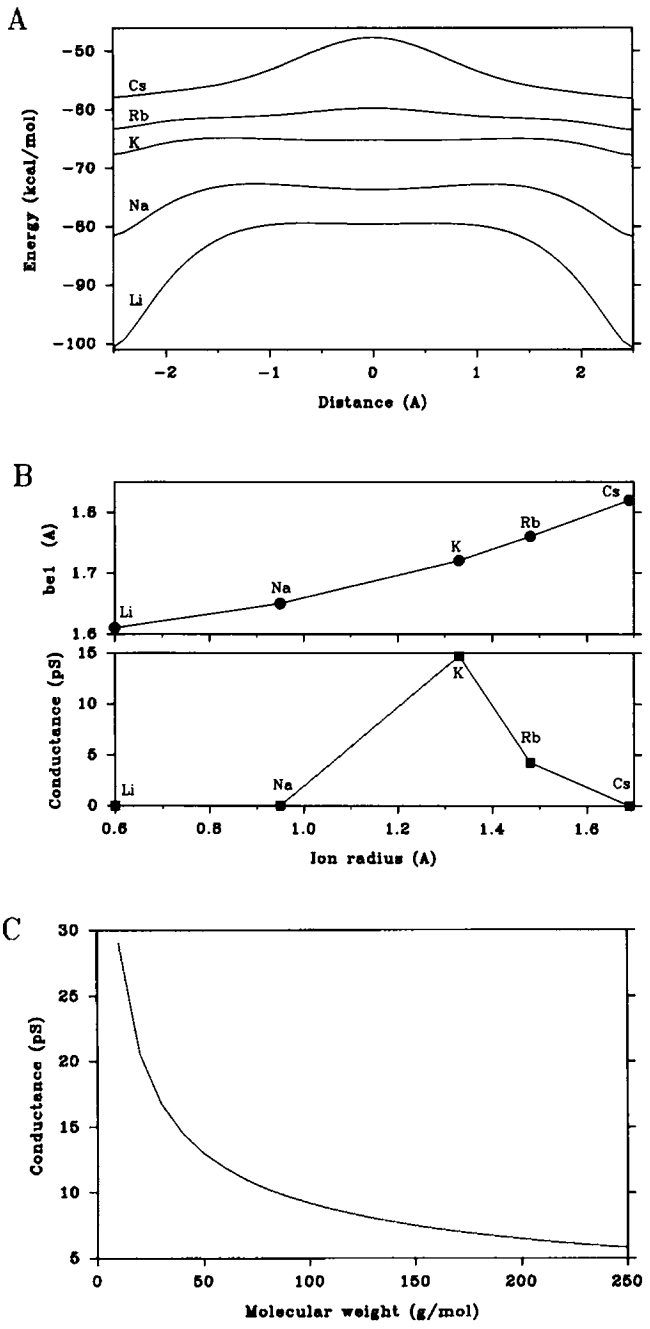

FIGURE 3 Effects of ion radius and mass on the energy profiles, the conductances, and the hydration. (*A*) The energy profiles of Li^+, Na^+, K^+, Rb^+, and Cs^+ in a K^+ channel calculated from Eq. 1, 10 mV across the selectivity filter. The energy was minimized at $x = -2.5$ Å and $x = 2.5$ Å. (*B*) Bottom, conductances corresponding to the above energy profiles plotted against ion radius, 100 mM salt on both sides. Top, effective water radius plotted against ion radius to assess the degree of hydration. (*C*) The conductances of hypothetical ions with a radius of 1.33 Å and a variable molecular weight from 10 to 250 g/mol.

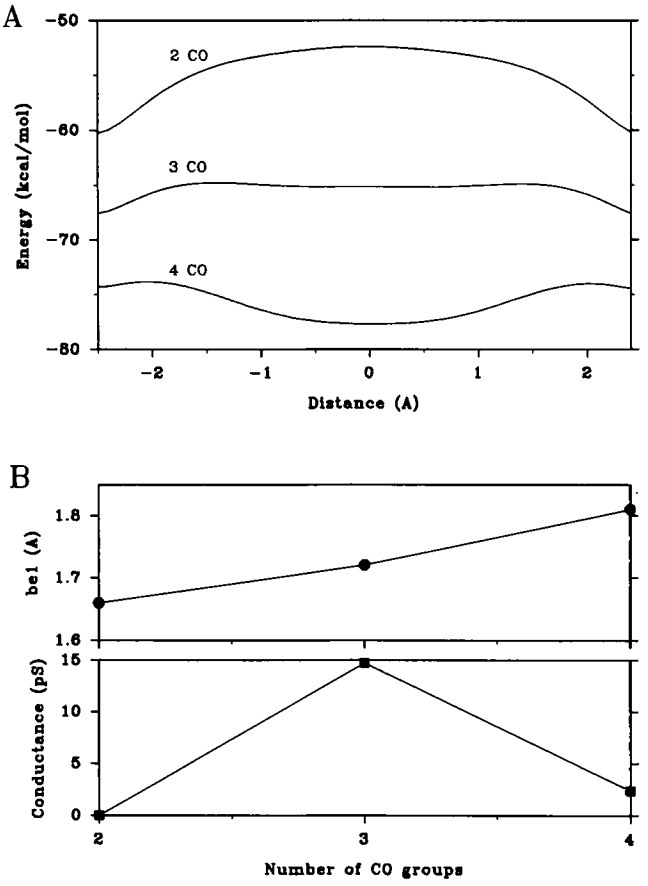

FIGURE 4 Effects of the number of site carbonyl groups (CO) on the K^+ energy profile, the conductances, and the hydration. (*A*) The energy profiles of K^+ with 2, 3, and 4 CO in a K^+ channel calculated from Eq. 1, 10 mV voltage across the selectivity filter. (*B*) Bottom, the conductances of above energy profiles plotted against the number of the site CO groups, 100 mM salt, and 10 mV voltage. Top, the effective water radius versus the number of site CO groups.

energy barrier is 7.86 kcal/mol because the dehydration energy is undercompensated by the Coulombic energy of interaction with the CO groups. The corresponding conductance is 0.0049 pS as shown in Fig. 4 *B* (*bottom*). For four CO groups, the dehydration energy is overcompensated. The deep central well makes a high-affinity binding site and tends to bind the ions tightly, which also leads to a decrease in channel conductance (2.37 pS). The appropriate compensation (3–3.5 CO groups) produces the maximum conductance (15 pS). Fig. 4 *B* also gives the effective equilibrium water radius b_{e1} as a function of the number of CO groups. The monotonic increase in b_{e1} with the increase in CO groups compared with nonmonotonic changes in conductance shows that elevation in the field strength of the sites indeed facilitates dehydration but not necessarily conductance.

Number of effective water dipoles determines hydration energy

The number of water dipoles (WD) associated with the ion at $-L$ and L may be dependent on the channel structure at $|x| > L$ (see Discussions). Fig. 5 *A* shows the energy profiles of K^+ in a K^+ channel, with the effective water dipole moment p varying from 2 to 3.5 WD. The total energy was minimized. As p increases, the first barrier (the compensated dehydration energy) also increases. The energy barrier corresponding to p = 2, 2.5, 3, and 3.5 WD is 0.022, 0.98, 2.81, and 5.61 kcal/mol, respectively. The corresponding conductance in Fig. 5 *B* is 2.59, 45.14, 14.71, and 0.22 pS. The degree of hydration can be assessed by the effective water radius b_{e1} which is reduced as the effective water dipole moment p increases (Fig. 5 *B*, *top*).

Channel radius cuts off ion permeation by ion radius

Fig. 6 *A* shows the energy profiles of K^+ in a K^+ channel calculated from Eq. 1. The total energy was minimized at $x = -2.5$ Å and $x = 2.5$ Å. The channel radius $R = (R_n - b)$ was varied from 1.2 to 1.8 Å. As the channel radius decreases, the central peak appears and becomes predominant as channel radius approaches 1.4 Å, due to the increase in short-range repulsive force. The corresponding conductances are shown in Fig. 6 *B* (*bottom*). The channel conductance is very small for a channel radius below 1.2 Å. The decrease in conductance for a larger channel radius results from less compensation of dehydration energy by farther CO groups. The monotonic decrease in the effective water radius b_{e1} in Fig. 6 *B* (*top*) is contributed by the reduction of site field strength.

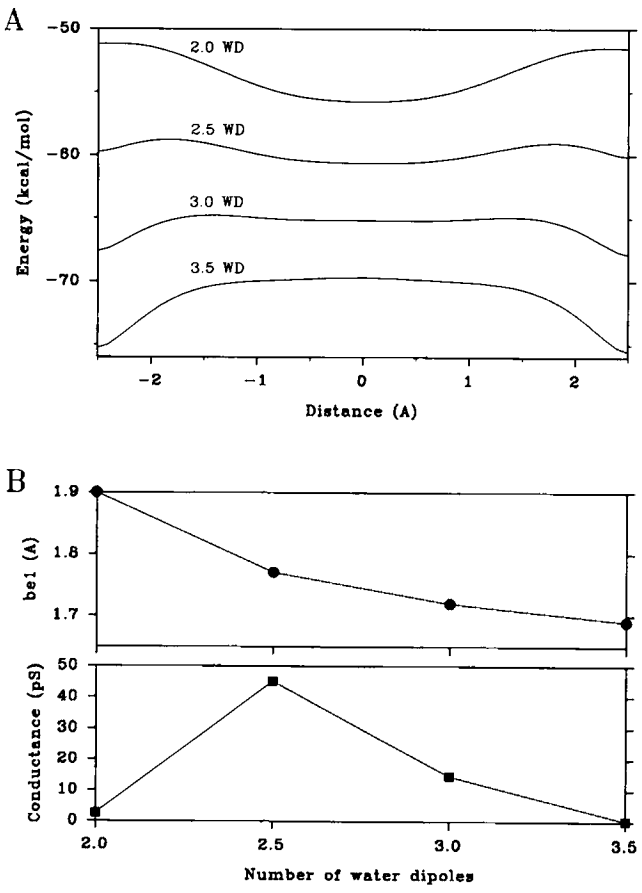

FIGURE 5 Effects of the number of the effective water dipoles (WD) on the K^+ energy profiles, the conductances, and the hydration. (*A*) The energy profiles of K^+ with 2, 2.5, 3, and 3.5 WD in a K^+ channel calculated from Eq. 1. (*B*) Bottom, the conductances corresponding to above energy profiles plotted against the number of WD, 100 mM salt, and 10 mV voltage. Top, the effective water radius versus the number of WD.

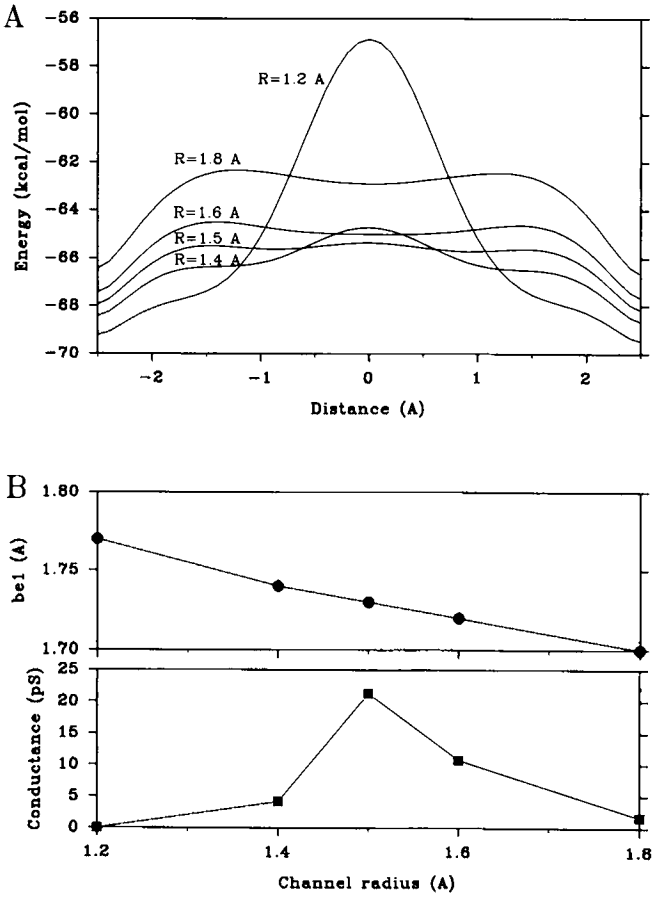

FIGURE 6 Effects of the channel radius on the K^+ energy profiles, the conductances, and the hydration. (*A*) The energy profiles of K^+ in a K^+ channel with the channel radius (R) of 1.2 Å, 1.4 Å, 1.5 Å, 1.6 Å, and 1.8 Å calculated from Eq. 1. (*B*) Bottom, the conductances corresponding to the above energy profiles plotted against channel radius, 100 mM salt, and 10 mV voltage. Top, the effective water radius versus the channel radius.

Current-voltage relations

The i–V curve of K^+ in a K^+ channel was calculated from Eq. 8 shown as the solid line in Fig. 7. The total energy was minimized at $x = -2.5$ Å and at $x = 2.5$ Å for each applied voltage. The energy barriers in Eq. 8 were calculated directly from the total energy for each voltage. The peak and well positions were not restricted to the fixed positions. The i–V curve is linear up to $\sim \pm 170$ mV with a zero voltage slope conductance of ~ 15 pS. The slight change in the slope at 100 mV is the point at which the two-peak energy profile is reduced to a one-peak energy profile, due to markedly elevated energy on side 1 and lowered energy on side 2. The dashed i–V curve in Fig. 7 was calculated from the voltage form of Eq. 10 with fixed peak and well positions. The energy profile was calculated from Eq. 1 while the applied voltage is zero. The i–V curve in this situation is approximately linear up to ± 50 mV with a zero voltage slope conductance of ~ 15 pS, then bends up from the voltage axis. That the two curves in Fig. 7 are similar in the low voltage range shows that the assumption of fixed peak and well positions is a good approximation under the weak external fields in deriving the voltage form of the current equation (Eq. 9).

Selectivity sequences

Fig. 8 *A* shows a semilogarithmic plot of single channel conductances of Li^+, Na^+, K^+, Rb^+, and Cs^+ versus channel radius calculated from Eq. 8. In these calculations the channel radius was varied from 0.5 to 2.2 Å.

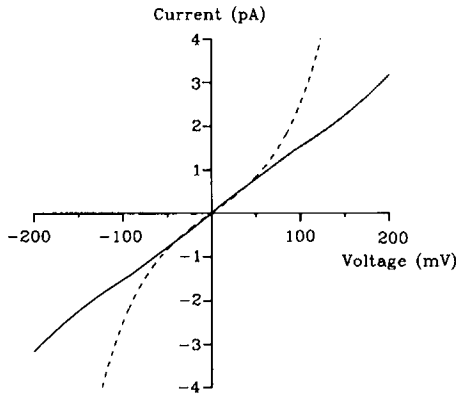

FIGURE 7 Current-voltage relations. (*Solid line*) The i–V curve of K^+ in a K^+ channel with voltage-dependent peak and well positions and with 100 mM symmetric solutions, calculated from Eq. 8. The energy profile was minimized at $x = -2.5$ Å and $x = 2.5$ Å for each voltage. (*Dashed line*) The i–V curve of K^+ in a K^+ channel with the fixed peak and well positions calculated from Eq. 10. The energy profile was calculated from Eq. 1 and minimized at $x = -2.5$ Å and $x = 2.5$ Å without applied field.

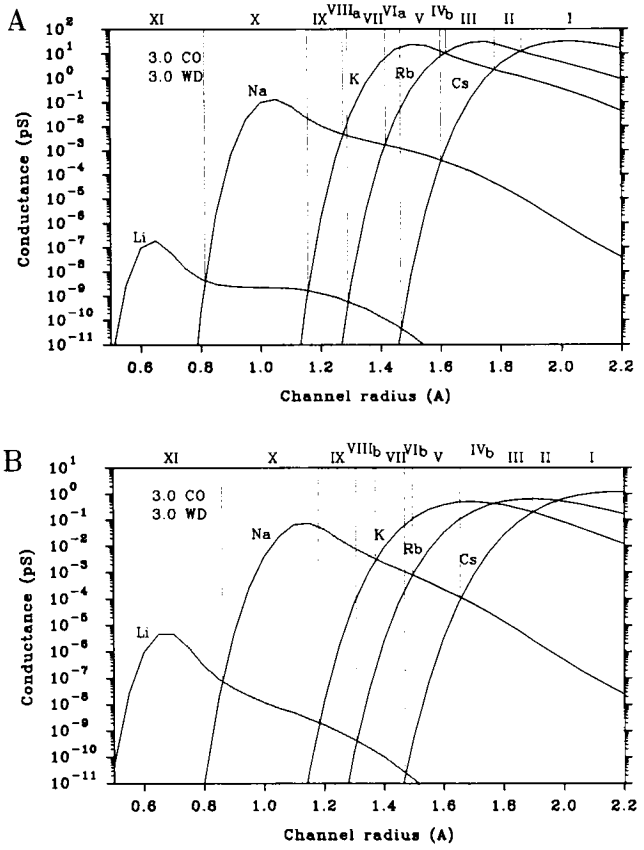

FIGURE 8 The selectivity sequence profiles defined by conductances versus the channel radius. (*A*) Semi-logarithmic plot of the single channel conductance versus the channel radius calculate from Eq. 8 with 100 mM salt and 10 mV voltage. The energy was minimized for each data point. The channel has three site carbonyl groups (CO) and three effective water dipoles (WD) as noted in the upper left corner of the graph. The selectivity sequences are named by the Roman numerals on the top of the horizontal axis. (*B*) Same plot as in *A* except that the power of short-range repulsive term is changed from 12 to 9.

The energy profile was minimized at $x = -2.5$ Å and at $x = 2.5$ Å for each data point. The selectivity sequence domains are separated by vertical dotted lines at the curve intersections. These sequences are named by successive Roman numerals on the top horizontal axis. There are 11 such conductance sequences for the channels with three CO groups and three WD. Further examining the intermediate three sequences, IV, VI, and VIII, I found that the relative positions of upper and lower intersections of these sequences are changeable under certain circumstances. A sequence with an upper intersection at the left (small channel radius) with respect to the lower intersection is named with the subscript a. A sequence with the reverse case is named with the subscript b. If those two intersections happen to

be at the same channel radius, the resulting sequence is degenerate. As the result of this nomenclature, the three intermediate sequences in Fig. 8 *A* are IV_b, VI_a, and $VIII_a$. It is apparent from this graph that the steepness of the rising phase of the conductance might alter the intermediate sequences. The steepness is determined by the power of the repulsive term of CO groups. To show the variations of the sequences, in Fig. 8 *B* the power of the repulsive term of CO groups in Eq. 1 is chosen to be 9 instead of 12. The twelfth power repulsion represents a fairly rigid channel selectivity filter. The ninth power can be interpreted as a relatively flexible channel. All other parameters are the same as those of Fig. 8 *A*. In Fig. 8 *B*, the relative positions of the intersections of the sequences VI and VIII are changed, which results in two more sequences, VI_b and $VIII_b$. From the changes in the relative positions of the intersections, a tentative conclusion can be drawn: sequences IV_a, VI_a, and $VIII_a$ result from rigid channels; sequences IV_b, VI_b, and $VIII_b$ are derived from relatively flexible channels.

To explore further how other channel structural parameters could modify conductances and conductance sequences, the number of CO and the number of WD were varied in Fig. 9, *A–D*. These include the low site-low water interactions (2 CO, 1.6 WD, Fig. 9 *A*), the low site-high water interactions (2 CO, 2.6 WD, Fig. 9 *B*), the high site-low water interactions (4 CO, 3.2 WD, Fig. 9 *C*), and the high site-high water interactions (4 CO, 4.2 WD, Fig. 9 *D*). The number of WD chosen for low water interactions is approximately the minimum number of water dipoles that the ion can hold at a reasonably short effective water radius (<4 Å) for Cs^+ during the energy minimization. Although the patterns of the conductances are similar for these four extreme permutations, there are several distinguishing features among them. Firstly, an increase in either field strength of the site or water interactions leads to general decreases in conductance for all ion species. The maximum conductance in the 2-CO and 1.6-WD channels is ~800 pS, and it drops off to ~1 pS in the 4-CO and 4.2-WD

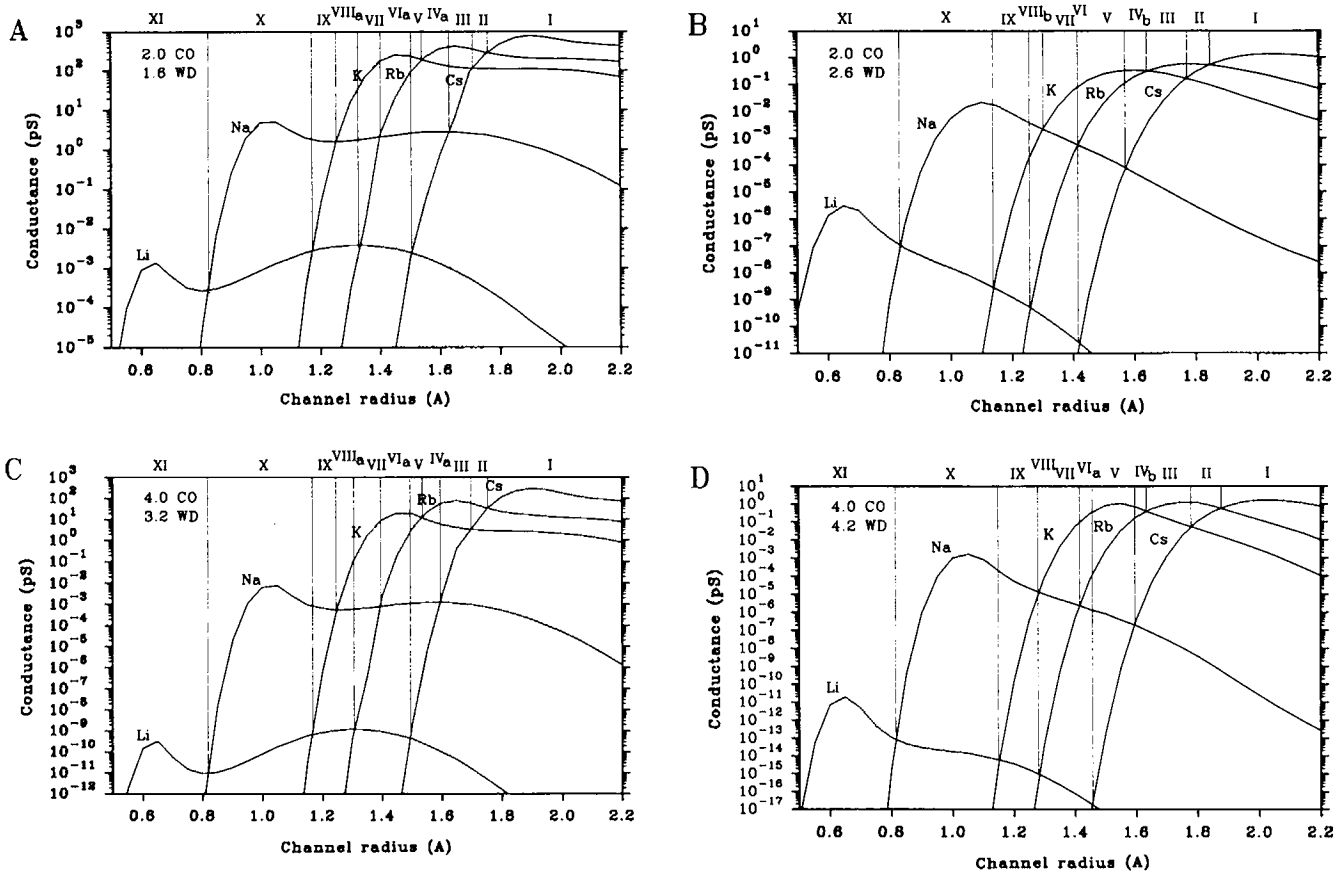

FIGURE 9 The selectivity sequence profiles for four extreme channel structures (all semi-logarithmic plots). The selectivity sequence profiles for the channels are shown with the following structures: (*A*) low site-low water interactions (2.0 CO, 1.6 WD). (*B*) low site-high water interactions (2.0 CO, 2.6 WD). (*C*) high site-low water interactions (4.0 CO, 3.2 WD). (*D*) high site-high water interactions (4.0 CO, 4.2 WD).

channels. Secondly, in the situation of low-water interactions, the K^+ and Rb^+ conductances approach the Cs^+ conductance at larger channel radii. Because K^+ has a lower ion mass and smaller radius, its average speed and effective cross-sectional area exceed those of Cs^+. It is not surprising that when the site and water interactions are reduced, the contributions of the average ion speed and the cross-sectional area of the channel to the conductance become predominant. Thirdly, increases in water interactions from Fig. 9 *A* to 9 *B* and from Fig. 9 *C* to 9 *D* lead to increases in the steepness of the falling phase of the conductances. As a result of these increases, the sequences IV_a, VI_a, and $VIII_a$ in Fig. 9 *A* are changed to the sequences IV_b, $VIII_b$, and a degenerate sequence IV in Fig. 9 *B*. Also, the sequences IV_a and $VIII_a$ in Fig. 9 *C* are changed to IV_b and a degenerate sequence VIII in Fig. 9 *D*. Therefore, those sequences with the subscript a are properties of channels with weak water interactions, and the sequences with subscript b are likely to be associated with channels involved in strong water interactions.

In summary, Figs. 8 and 9 demonstrate a total of 14 conductance sequences. The sequences IV_a, VI_a, and $VIII_a$ can result from channels with weak water interactions and/or rigid selective filters. The sequences IV_b, VI_b, and $VIII_b$ can be found in channels with strong water interactions and/or flexible selectivity filters. Furthermore, the two intersections of the sequence V in Fig. 9 *A* are very close. It is possible that under the condition of very weak water interactions and/or very rigid selectivity filter, this sequence can be altered to a new sequence, V_c (Rb > K > Na > Li > Cs, not shown in graphs). Thus, the number of total possible sequences grows to 15. To distinguish them from the Eisenman equilibrium binding selectivity sequences, these conductance sequences are named as "kinetic selectivity sequences" and are listed in Table 2. Ten of these are identical with the sequences derived by Eisenman (1962). However, IV_a, V_c, VI_a, VII, and $VIII_a$ are new. The Eisenman sequence Na > K > Rb > Cs > Li is absent in this analysis. These 15 selectivity sequences are the result of a single selectivity filter. Multiple heterogeneous selectivity filters may yield more complicated selectivity sequences.

TABLE 2 Kinetic selectivity sequences

I	Cs > Rb > K > Na > Li		
II	Rb > Cs > K > Na > Li		
III	Rb > K > Cs > Na > Li		
IV_a	Rb > K > Na > Cs > Li	IV_b	K > Rb > Cs > Na > Li
V	K > Rb > Na > Cs > Li	V_c	Rb > K > Na > Li > Cs
VI_a	K > Rb > Na > Li > Cs	VI_b	K > Na > Rb > Cs > Li
VII	K > Na > Rb > Li > Cs		
$VIII_a$	K > Na > Li > Rb > Cs	$VIII_b$	Na > K > Rb > Li > Cs
IX	Na > K > Li > Rb > Cs		
X	Na > Li > K > Rb > Cs		
XI	Li > Na > K > Rb > Cs		

DISCUSSION

This study has attempted to link measurable single channel currents to microscopic parameters of ions and the selectivity filter. While precise details of ionic pore structures are not yet known, several studies implicate a role for carbonyl and carboxyl groups (Bezanilla and Armstrong, 1972; Hille, 1971). In this work I have tested models of selectivity filters lined with a symmetric arrangement of carbonyl groups. By varying the structural parameters of the pore it has been possible to match experimental data regarding conductances. The importance of Imoto and colleagues' (1988) findings to the present work is twofold. First, it provides a structural basis for the derivation of a detailed energy function. Second, the axial symmetry of charge distributions markedly simplifies the energy function. A direct application of molecular kinetic theory using the Maxwellian and Boltzmann distributions has been proven to have some advantages over ERT. In developing a new approach it is necessary that the resulting flux or current equation leads directly to the Nernst and GHK equation. This has been demonstrated in this work. In the original formulation of the GHK equation the permeability was defined in terms of ion mobility in the membrane. In the present work the permeability has been defined by microscopic parameters only, e.g., molecular weight, channel cross-sectional area, and energy profiles. Further, as defined here, permeabilities can be expressed in terms of experimentally measurable quantities (Eqs. 9 and 11).

Current-voltage relations

The i–V curve of the GHK voltage equation derived from the constant field solution of the Nernst-Plank equation for symmetric solutions is linear. The same result can be derived also from ERT with an infinite number of barriers. For the energy profiles with two energy barriers and fixed positions of energy barrier and well, both Nernst-Planck theory and ERT give superlinear i–V curves (Cooper et al., 1985). Similarly, in Fig. 7, the i–V curve (*dashed line,* calculated from Eq. 10) with fixed barrier and well positions shows superlinearity beyond ±50 mV. However, without the constraint of fixed energy barrier and well positions, the i–V curve in Fig. 7 (*solid line,* calculated from Eq. 8) shows approximately linear behavior up to ±170 mV. Alternation of ion or channel parameters may also produce sublinear

curves at some voltage ranges (data not shown). The slopes of two curves at a voltage range below ±50 mV are identical. This result demonstrates that the assumption of fixed energy barrier and well positions is a good approximation only at low voltage. Several interesting experimental results in Ca^{++} activated K^+ channels show that the i–V curve for K^+ and Tl^+ are sublinear and for Rb^+ and NH_4^+ are superlinear (Yellen, 1984; Eisenman et al., 1986). It is found in the present work that this linearity is very sensitive to the changes of local energy profiles for specific ion species, and also to the voltage dependence of positions of energy minima and maxima. The latter dependence originates from the voltage sensitivity of b_{e1} and b_{e2} during energy minimization. While a positive voltage is applied, the effective water dipole at side 1 is forced to move closer to the ion and that at side 2 farther from the ion. Thus the positions of the energy minima and maxima change with the applied voltage. In actual channels the distance for the ion to separate from the effective water dipoles ($-L$ and L) also may be voltage dependent. This dependence is neglected in this study.

Kinetic selectivity sequences

One of the predictions from this model is that there is a total of 15 possible selectivity sequences for ion channels with one selective filter. For a given channel structure, if only channel radius is varied, the number of selectivity sequences is reduced to 11. 10 of these 15 sequences are the same as, but 5 intermediate sequences differ from, the Eisenman sequences. These results confirm that any two of the so-called asymmetrical interactions with ions will yield 11 selectivity sequences in terms of free energy (Eisenman, 1962). Two major such interactions recognized in this work are the ion-water interactions and the short-range repulsive interactions between the ions and the selectivity filter. These two interactions depend differently on ion size. In the channels with large radii, the ion-water interactions are predominant, yielding sequence I. For those channels with small radii, the steep short-range repulsive interactions take over and eventually reverse the sequence from I to XI. The concept of ion-water and short-range repulsive interactions as the major cause of selectivity contradicts equilibrium binding selectivity theory in which selectivity is purely accounted for by ion-water and ion-site Coulombic interactions. The results in Fig. 9 show that the field strength of the site alters the absolute level of conductances for all ion species but does not markedly change the patterns of selectivity sequences. Another discrepancy between the present work and binding selectivity theory is that both the ion mass and the effective channel cross-sectional area are found in this model to modify the conductances and selectivity sequences. In the present theory, the rate of ions that strike the channel opening is proportional to the channel cross-sectional area and the average ion speed. The latter is inversely proportional to the square root of ion mass. The theory thus predicts that since Tl^+ and K^+ have similar crystal radii their energy profiles and the channel cross-sectional areas might be similar in a K^+-like channel, so using Eq. 8 their conductance ratio should approximately equal $(m_K/m_{Tl})^{1/2} = 0.44$ (see also Fig. 3 *C*). A ratio of 0.41 is found experimentally in the Ca^{++}-activated K^+ channel (Eisenman et al., 1986). This close agreement could, however, be fortuitous. To distinguish further among different theories of selectivity will require additional experimentations. Due to the signal-to-noise ratio limitations, very few conductance sequences for all five alkali cations have been successfully measured in symmetric solutions (Latorre and Miller, 1983). The conductance sequences of the EIM channel (Cs > Rb > K > Na > Li, Latorre and Alvarez 1981), and that of the gramicidin A channel (Rb > Cs > K > Na > Li, Hladky and Haydon 1972; Neher et al., 1978) and porin (Benz et al., 1980) are consistent with the Eisenman theory and also with the kinetic selectivity sequence I and II, respectively. The results of single channel conductance studies of the sarcoplasmic reticulum K^+ (SR-K) channel (Coronado et al., 1980; Labarca and Miller, 1981) reveal an interesting sequence: K > Rb > Na > Li > Cs. This sequence does not fall into any of the 11 Eisenman sequences but follows the sequence VI_a of the kinetic selectivity sequences in the category of ion channels with low water interactions and/or rigid selectivity filter.

Structural implications

The potential energy function ascribed to carbonyl groups in this work should not be mistaken to have a direct structural implication. It suggests only that the field strength of the selectivity filter is equivalent to that number of carbonyl groups standing in free space; and each carbonyl group is idealized as two separated point charges with opposite signs. The actual selectivity filter might be formed by carboxyl groups or other kinds of negative charges, but they are subject to be modified to reduce their field strength. The dielectric constant of lipid hydrocarbon as determined by low-frequency impedance measurements is 2.2. (Ashcroft et al., 1983); and that of channel protein is ~3–5 (Honig, 1986). These two surrounding media obviously reduce the field strength of the functional groups. It is also found that positively charged groups in the vicinity of the negative functional charges may contribute to the modification of the field strength (Imoto et al., 1988). Before these

modifications are specified, the use of carbonyl groups in free space as an assessment for the field strength is convenient. In real K^+ channels, the conductances may range from a few pS to hundreds of pS. One feature demonstrated in Fig. 9 is that the maximum conductance can be regulated by the site field strength of the selectivity filter. The distribution and number of positive charges adjacent to the selectivity filter (Imoto et al., 1988) could be responsible for the modification of maximum conductance. From the maximum conductances of Na^+ and K^+ in Fig. 9, it can be further suggested that if a Na^+ channel has the same conductance as a K^+ channel, the field strength of the former is expected to be lower than that of the latter.

The regulation of maximum conductances is even more prominent by altering the number of effective water dipoles as in Fig. 9. I consider that this regulation can be achieved by changing the geometry of the channel mouth as illustrated in Fig. 10. The type I channel has a short tunnel (a narrow part of the channel where ions undergo single-file movements) with one adjacent water dipole toward the ion. The directions of the water dipoles in the mouth are disrupted by random motions of water molecules. The type II channel has a wide mouth which allows the ion access to several water dipoles. The type III channel has a long tunnel which facilitates the alignment of water dipoles toward the ion (Kim et al., 1985). The latter two types of channels are expected to be higher in water interactions. The polar groups in the channel wall might reduce the water interactions by disorienting the water dipoles.

The level of selectivity among different ions is regulated by the rigidness and field strength of the selectivity filter, and also the number of effective water dipoles.

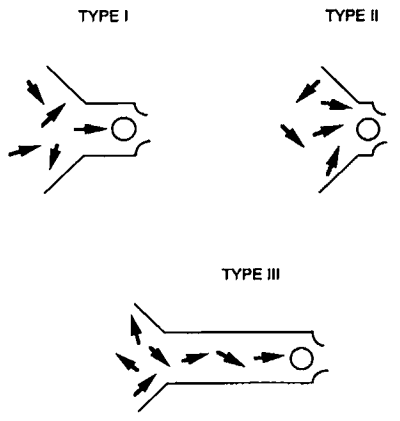

FIGURE 10 Correlations of channel geometry and the number of effective water dipoles. The circle represents the ion in the tunnel and arrows denote the directions of water dipoles. Type I, short tunnel; Type II, wide access; Type III, long tunnel.

The first of these is determined by the power of the repulsive term which is chosen to be 12 in the present work. Due to this choice, the rising phase of the conductances in Fig. 9 appears too steep in comparison with published experimental results. It is likely that in actual channels fluctuations of the structure of the selectivity filter cannot be neglected. The twelfth power of the repulsive term in this model thus may be overestimated. Taking the K^+ channel as an example, the power of the repulsive term should be fitted by the Rb^+ and Cs^+ conductances from experiments. The second factor influencing the steepness of the selectivity is the surrounding medium which reduces the field strength of the site. A simple way to evaluate this effect is to introduce a dielectric constant >1. Increasing this constant from 1 to 5 significantly reduces the steepness of the selectivity (data not shown here). The sharpness of differences in conductances among small cations, e.g., Li^+ and Na^+, relates to ion-water interactions. It can be observed from Fig. 9 that the higher the ion-water interactions the steeper is this selectivity dependence. In this approach, the number of effective water dipoles is assumed to be independent of ion species. This may not be the case for small ions in large channels because an adjacent water molecule may cross the selectivity filter without separation from the ion. Thus the conductance for small ions in large channels may be underestimated in this work.

Choice of parameters and assessment of assumptions

The microscopic model in the present work does not contain any free macroscopic parameters. Despite the uncertainty of the values of some microscopic parameters, discussions of their range might provide structural information about the molecular mechanism of selective permeation of ion channels. The distance for the ion to separate from the water dipoles was chosen to be 2.5 Å for all ion species. The argument for this choice is that for the selectivity filter to strip off the hydration sphere, this distance should approximately equal the sum of the Van der Waals' radius of the carbonyl oxygen (1.4 Å) and the average dimensions of alkali cations. Because the distance of separation itself is a fuzzy concept, 2.5–3.0 Å as an average for all ion species is not unreasonable. More accurate analysis requires that this parameter be finely adjusted for the ions with different size. In studies of channel block by impermeant cations, it is found that the apparent electrical distance is linearly correlated with ion size (French and Shoukimas, 1985; Ravindran et al., 1991). It appears that small cations, Li^+ and Na^+, approach the narrowest region more closely than Cs^+. If this is indeed the case, the dehydration

energy for Li^+ and Na^+ may be overestimated in this work.

The use of the Maxwellian and Boltzmann distributions requires that the system is in the equilibrium state. This condition generally is not satisfied in a transport system. However, if the flux of ions is low enough in comparison with bath solutions so that the changes in spatial distribution of ions are negligible during the period of measurement, then ion distributions in each compartment can be considered to be in quasi-equilibrium (Cooper et al., 1988). Under this condition, the Maxwellian and Boltzmann distributions are still applicable. In symmetrical solutions with low applied voltage, this state is more likely to be reached.

In the treatment of ions passing over barriers, it is assumed that an ion undergoes no collisions during the passage (the ballistic crossing assumption; Cooper et al., 1988). The distance for crossing a barrier in this work is ~1.0–2.5 Å as shown in Fig. 3*A*. If the mean free path (MFP) of water molecules in the channel is comparable to this distance, then the fluctuations around the MFP can bring a large number of opportunities for collision-free transitions. The MFP of bulk water molecules is 0.69 Å (MFP = $0.056/b_w^2C_w$, where C_w = 55.6 M/l is the density of bulk water; Loeb, 1934). At the interior of an ion channel the MFP of water could be quite different from that in bulk solutions. I have analyzed ion-water interactions and found that to fit experimental results, the water density within the channel must be far lower than that in bulk solutions. Two mechanisms possibly contribute to this reduction. First, the image potential exerted by the surrounding media may prevent a fraction of water molecules from entering the channel. Second, the polar channel wall may substitute for part of water molecules of hydration surrounding a cation. The reduction of water molecules within the channel serves to increase the MFP of ions in the channel. An average of five water molecules has been indirectly measured in gramicidin A channels (Rosenberg and Finkelstein, 1978). This suggests that if the channel is 25 Å in length and 4 Å in diameter (Urry, 1971), then the water density in the channel is 26.4 M/l and the corresponding MFP is 1.45 Å. Similar measurements in SR-K channels suggest an average of 2.3 water molecules in the tunnel (Miller, 1982*a*). Provided that 10 Å of the tunnel length and 7 Å of the diameter are independently probed by quaternary ammonium blockers (Miller, 1982*b*), the MFP in SR-K channel is estimated to be 3.85 Å. The MFP's of both cases are very close to the distance for crossing the barrier, which suggests that the ballistic crossing assumption used in this work holds within channels.

The near-axis approximation is appropriate for axially symmetric carbonyl groups and a relatively small channel radius for the following two reasons. First, the off-axis energy drop is similar to a gradual elliptical function resulting from axial symmetry. Second, the short-range interactions are elevated to flatten the energy drop while the ion approaches a carbonyl oxygen. If carbonyl groups are asymmetrically distributed, as in the gramicidin A channel (Schröder, 1985*a*), or one of the carbonyl groups is replaced by a charged carboxyl group, or the channel radius is very large, off-axis ion movement can no longer be neglected. In these situations, the small ions, e.g., Li^+ or Na^+ will be translocated through an optimal off-axis path and their conductances may decrease. However, the deviations in magnitude of conductances do not likely affect the general conclusions on the selectivity sequences in this work.

I am grateful to Dr. P. Shrager for his continuous encouragement and help in computer modeling and preparing the manuscript. I also wish to thank Drs. R. A. Eatock and T. Begenisich for their critical comments on the manuscript.

Received for publication 10 September 1990 and in final form 7 February 1991.

REFERENCES

Ashcroft, R. G., H. G. L. Coster, D. R. Laver, and J. R. Smith. 1983. The effects of cholesterol inclusion on the molecular organization of bimolecular lipid membranes. *Biochim. Biophys. Acta.* 730:231–238.

Benz, R., K. Janko, and P. Laüger. 1980. Pore formation by the matrix protein (porin) of *Escherichia coli* in planar bilayer membranes. *Annu. NY Acad. Sci. USA.* 258:13–24.

Bezanilla, F., and C. M. Armstrong. 1972. Negative conductance caused by entry of sodium and cesium ions into the potassium channels of squid axons. *J. Gen. Physiol.* 60:588–608.

Born, M. 1920. Volumen und Hydratationswärme der Ionen. *Z. Phys.* 1:45–48.

Cooper, K. E., E. Jakobsson, and P. G. Wolynes. 1985. The theory of ion transport trough membrane channels. *Prog. Biophys. Molec. Biol.* 46:51–96.

Cooper, K. E., P. Y. Gates, and R. S. Eisenberg. 1988. Diffusion theory and discrete rate constants in ion permeation. *J. Membr. Biol.* 106:95–105.

Coronado, R., R. L. Rosenberg, and C. Miller. 1980. Ionic selectivity, saturation, and block in a K^+-selective channel from sarcoplasmic reticulum. *J. Gen. Physiol.* 76:425–446.

Eisenman, G. 1962. Cation selective glass electrodes and their mode of operation. *Biophys. J.* 2(Suppl. 2):259–323.

Eisenman, G., and S. Krasne. 1975. The ion selectivity of carrier molecules, membranes and enzymes. *In* MTP International Review of Science, Biochemistry Series. C. F. Fox, editor. Butterworths, London. 2:27–59.

Eisenman, G., R. Latorre, and C. Miller. 1986. Multi-ion conduction and selectivity in the high-conductance Ca^{++}-activated K^+ channel from skeletal muscle. *Biophys. J.* 50:1025–1034.

French, R. J., and J. Shoukimas. 1985. An ion's view of the potassium channel. The structure of the permeation pathway as sensed by a variety of blocking ions. *J. Gen. Physiol.* 85:669–698.

Goldman, D. E. 1943. Potential, impedance and rectification in membranes. *J. Gen. Physiol.* 27:37–60.

Hille, B. 1971. The permeability of the sodium channel to organic cations in myelinated nerve. *J. Gen. Physiol.* 27:37–60.

Hille, B. 1972. The permeability of the sodium channel to metal Cations in myelinated nerve. *J. Gen. Physiol.* 59:637–658.

Hille, B. 1973. Potassium channels in myelinated nerve: selective permeability to small cations. *J. Gen. Physiol.* 61:669–686.

Hille, B. 1975. Ionic selectivity of Na and K channels of nerve membranes. *In* Membranes—A Series of Advance. Lipid Bilayers and Biological Membranes: Dynamic Properties. G. Eisenman, editor. Marcel Dekker, New York. 3:255–323.

Hille, B. 1984. Ionic Channels of Excitable Membranes. Sinauer Associates, Inc., Sunderland, MA. 166 pp.

Hladky, S. B., and D. A. Haydon. 1972. Ion transfer across lipid membranes in the presence of gramicidin A. *Biochim. Biophys. Acta.* 274:294–312.

Hodgkin, A. L., and B. Katz. 1949. The effect of sodium ions on the electrical activity of the giant axon of the squid. *J. Physiol.* 108:37–77.

Honig, B. 1986. Electrostatic interactions in membranes and proteins. *Annu. Rev. Biophys. Chem.* 15:163–193.

Imoto, K., C. Busch, B. Sakmann, M. Mishina, T. Konno, J. Nakai, H. Bujo, Y. Mori, K. Fukuda, and S. Numa. 1988. Rings of negatively charged amino acids determine the acetylcholine receptor channel conductance. *Nature (Lond.).* 335:645–648.

Kim, K. S., D. P. Vercautern, M. Welti, S. Chin, and E. Clementi. 1985. Interaction of K^+ ion with the solvated gramicidin A transmembrane channel. *Biophys. J.* 47:327–335.

Kostyuk, P. G., and O. A. Krishtal. 1977. Separation of sodium and calcium currents in the somatic membrane of molluscan neurones. *J. Physiol. (Lond.).* 270:545–568.

Labarca, P. P., and C. Miller. 1981. A K^+-selective, three-state channel from fragmented sarcoplasmic reticulum of frog leg muscle. *J. Membr. Biol.* 61:31–38.

Latorre, R., and O. Alvarez. 1981. Voltage-dependent channels in planar lipid bilayer membrane. *Physiol. Rev.* 61:77–150.

Latorre, R., and C. Miller. 1983. Conductance and selectivity in potassium channels. *J. Membr. Biol.* 71:11–30.

Läuger, P. 1973. Ion transport through pores: a rate-theory analysis. *Biochim. Biophys. Acta.* 311:423–441.

Läuger, P. 1982. Microscopic calculation of ion-transport rates in membrane channels. *Biophys. Chem.* 15:89–100.

Loeb, L. B. 1934. The Kinetic Theory of Gases. McGraw-Hill Book Company, Inc., New York. 97 pp.

Mackey, M. C. 1971. Kinetic theory model for ion movement through biological membranes II. Interionic selectivity. *Biophys. J.* 11:91–97.

Miller, C. 1982*a*. Coupling of water and ion fluxes in a K^+-selective channel of sarcoplasmic reticulum. *Biophys. J.* 38:227–230.

Miller, C. 1982*b*. *Bis*-quaternary ammonium blockers as structural probes of the sarcoplasmic reticulum K^+ channel. *J. Gen. Physiol.* 97:869–891.

Mullins, L. J. 1959. Ion selectivity of carriers and channels. *Biophys. J.* 15:921–931.

Neher, E. J. Sandblom, and G. Eisenman. 1978. Ion selectivity, saturation, and block in gramicidin A channels. *J. Membr. Biol.* 40:97–116.

Parlin, R. B., and H. Eyring. 1971. Membrane permeability and electrical potential. *In* Ion Transport Across Membranes. M. T. Clarke, editor. Academic Press, New York. 103–118.

Ravindran, A., L. Schild, and E. Moczydlowski. 1991. Divalent cation selectivity for external block of voltage-dependent Na^+ channels prolonged by batrachotoxin. Zn^+ induces discrete substrates in cardiac Na^+ channels. *J. Gen. Physiol.* 97:89–115.

Rosenberg, P., and A. Finkelstein. 1978. Water permeability of gramicidin A-treated lipid bilayer membranes. *J. Gen. Physiol.* 72:341–350.

Schröder, H. 1985*a*. A molecular model for ion selectivity in membrane channels. *Eur. Biophys. J.* 11:157–165.

Schröder, H. 1985*b*. Rate theoretical analysis of ion-selectivity in membrane channels with elastically bound ligands. *Eur. Biophys. J.* 12:129–142.

Seitz, F. 1940. The Modern Theory of Solids. McGraw-Hill Book Company, Inc., New York. 79 pp.

Urry, D. W. 1971. The gramicidin A transmembrane channel: a proposed $\pi_{(L,D)}$ helix. *Proc. Natl. Acad. Sci. USA.* 68:672–676.

Woodbury, J. W. 1971. Eyring rate theory model of the current-voltage relationships of ion channel in excitable membranes. *In* Chemical Dynamics: Papers in Honor of Henry Eyring. J. O. Hirschfelder, editor. John Wiley, New York. 601–617.

Wu, J. 1991. Fifteen selectivity sequences in channels revealed by a microscopic model. *Biophys. J.* 59:18*a*. (Abstr.)

Yellen, G. 1984. Ionic permeation and blockade in Ca^{++}-activated K^+ channels of bovine chromaffin cells. *J. Gen. Physiol.* 84:157–186.